Scalar-sector extensions in light of the LHC data

Bohdan GRZADKOWSKI
University of Warsaw

- The LHC data
- Gravity-Higgs mixing (the off-brane RS setup)
  - The model
  - Results
- Second Higgs doublet
  - Type I and II models
  - Strategy: scanning and experimental constraints
  - Results
- Summary

◇ B.G., J. F. Gunion and M. Toharia, "Higgs-Radion interpretation of the LHC data?" Phys. Lett. B **712**, 70 (2012),
◇ D. Dominici, B.G., J. F. Gunion and M. Toharia, "The Scalar sector of the Randall-Sundrum model", Nucl. Phys. B **671**, 243 (2003),
◇ A. Drozd, B.G., J. Gunion and Y. Jiang, "Two-Higgs Doublet Models and Enhanced Rates for a 125 GeV Higgs", in progress.

The LHC data

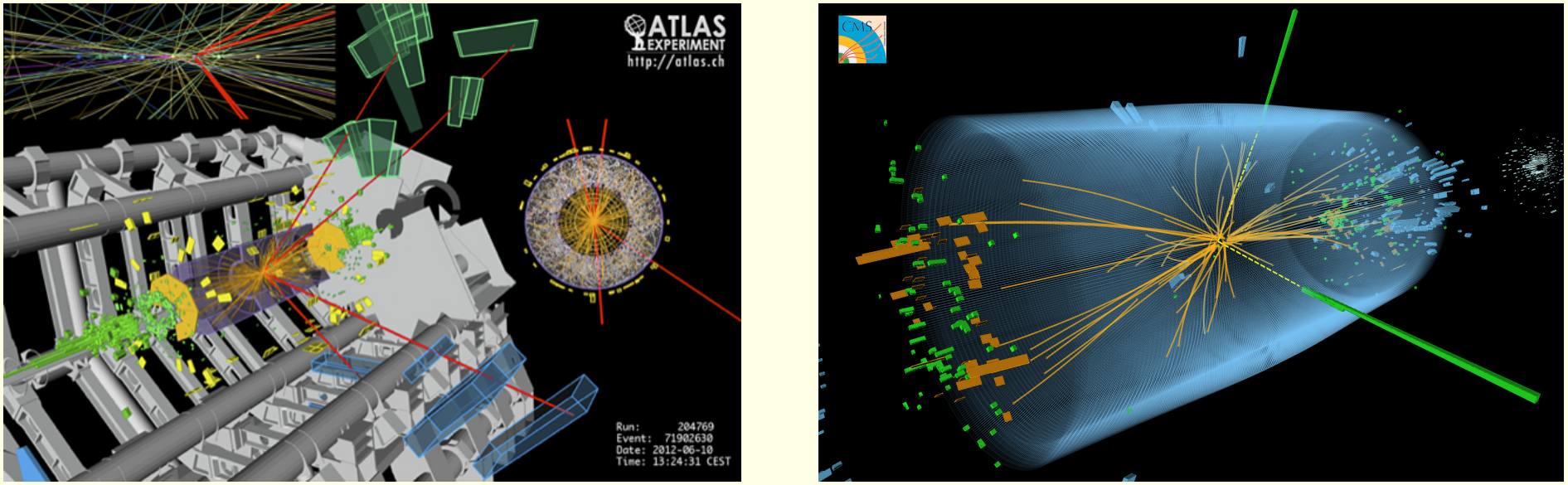

Figure 1: 1) Candidate Higgs Decay to four muons ($h \to ZZ \to 4\mu$) recorded by ATLAS in 2012. 2) Event recorded by CMS in 2012. The event shows characteristics expected from a decay of the SM Higgs boson to a pair of photons (dashed yellow lines and green towers): $h \to \gamma\gamma$.

- G. Aad *et al.* [ATLAS Collaboration], "Observation of a new particle in the search for the Standard Model Higgs boson with the ATLAS detector at the LHC", [arXiv:1207.7214 [hep-ex]].
- S. Chatrchyan *et al.* [CMS Collaboration], "Observation of a new boson at a mass of 125 GeV with the CMS experiment at the LHC", [arXiv:1207.7235 [hep-ex]].

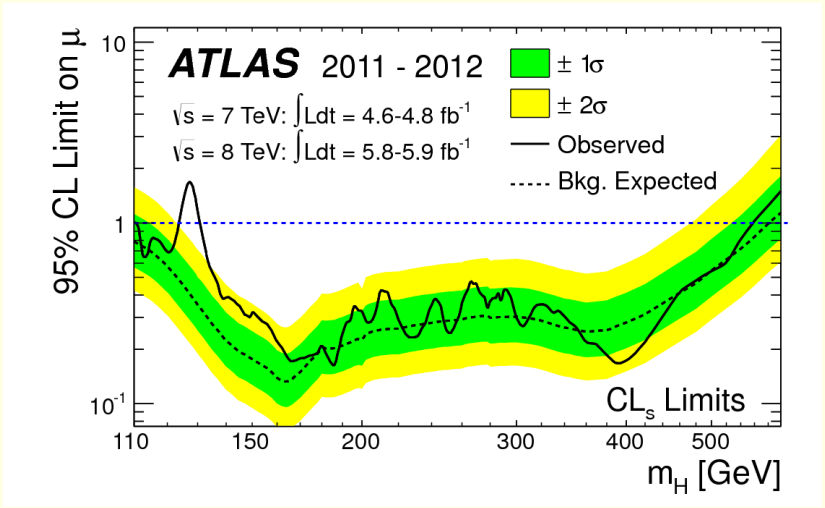

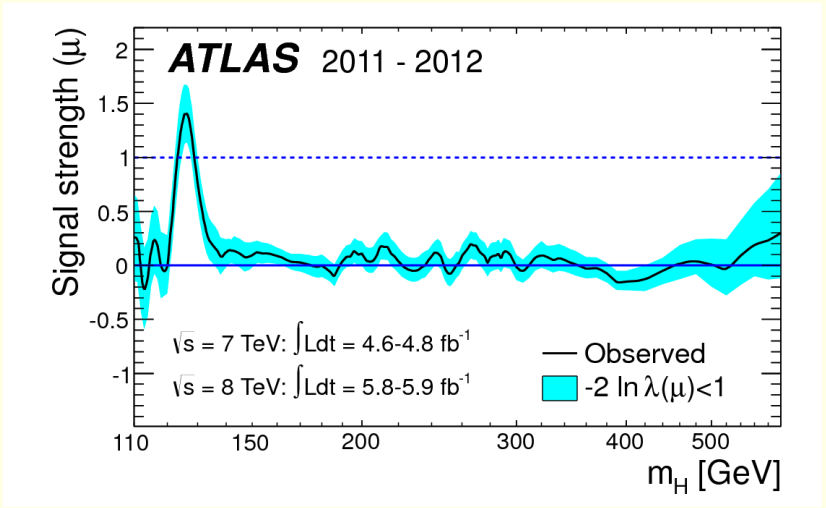

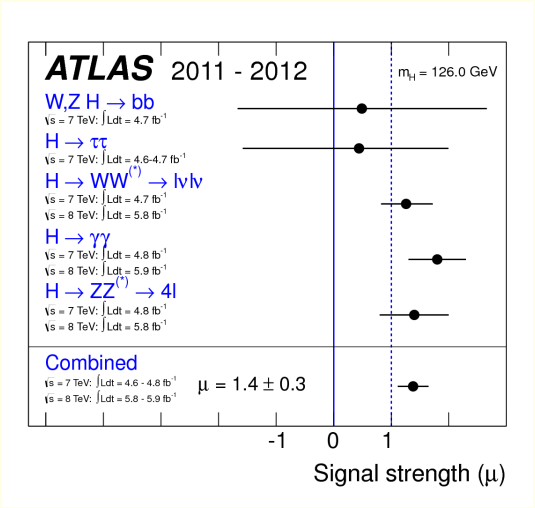

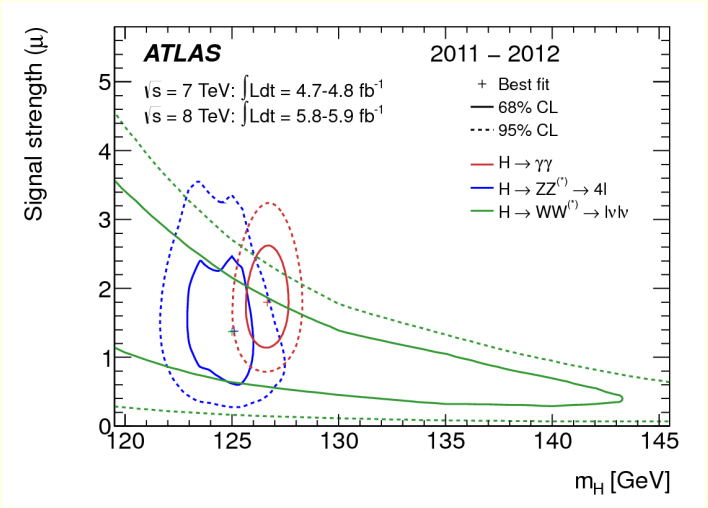

Figure 2: 1) The observed (solid) 95% CL upper limit on the signal strength as a function of m_h and the expectation (dashed) under the background-only hypothesis. The green and yellow bands show the $\pm 1\sigma$ and $\pm 2\sigma$ uncertainties on the background-only. 2) The best-fit signal strength μ as a function of m_h. The band indicates the approximate 68% CL interval around the fitted value. 3) Measurements of the signal strength parameter μ for $m_h = 126$ GeV for the individual channels and their combination. 4) Confidence intervals in the (μ, m_h) plane for the $h \to ZZ^{(*)} \to 4l$, $h \to \gamma\gamma$, and $h \to WW^{(*)} \to l\nu l\nu$ channels, including all systematic uncertainties. The markers indicate the maximum likelihood estimates in the corresponding channels.

Gravity-Higgs mixing (the off-brane RS setup)

- 3 space, 1 time (x^μ), + 1 extra spatial dimension (y), orbifold: $y \equiv y+1$, $y \equiv -y$
- Standard Model particles on a "visible" brane (at $y = 1/2$),
- Planck mass scale physics on the "hidden" (at $y = 0$),
- Gravity in the bulk (for any y),

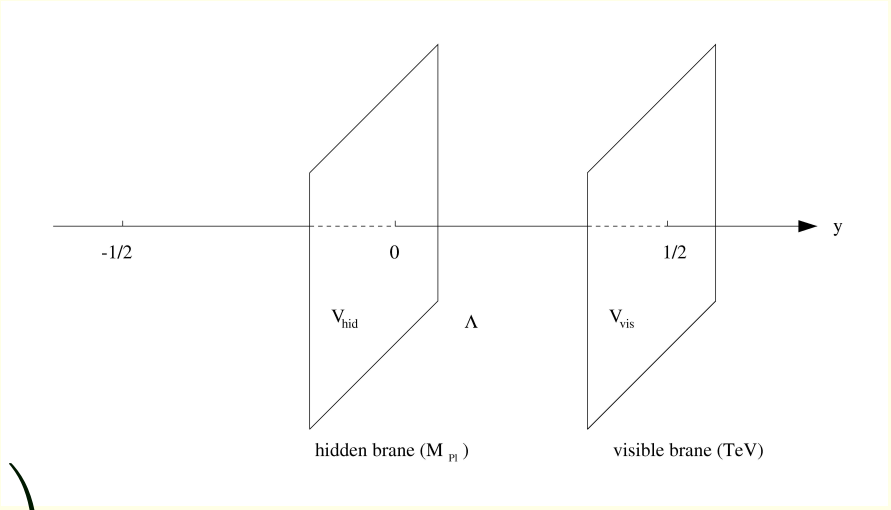

The full 5d action ($\epsilon^2 \equiv m_{Pl5}^{-3}$):

$$S = -\int d^4x\, dy \sqrt{-\widehat{g}} \left(\frac{\widehat{R}}{\epsilon^2} + \Lambda \right) + \int d^4x \sqrt{-g_{\rm hid}} (\mathcal{L}_{\rm hid} - V_{\rm hid}) + \int d^4x \sqrt{-g_{\rm vis}} (\mathcal{L}_{\rm vis} - V_{\rm vis})$$

Strategy:

- Solution of the Einstein's equations:

$$ds^2 = e^{-2m_0 b_0 |y|} \eta_{\mu\nu} dx^\mu dx^\nu - b_0^2 dy^2$$

for

$$V_{\rm hid} = -V_{\rm vis} = \frac{12 m_0}{\epsilon^2} \qquad \text{and} \qquad \Lambda = -\frac{12 m_0^2}{\epsilon^2}$$

- An expansion around the background metric:
  - $\eta_{\mu\nu} \to \eta_{\mu\nu} + \epsilon h_{\mu\nu}(x,y)$,
  - $b_0 \to b_0 + b(x)$,

$$h_{\mu\nu}(x,y) = \sum_n h^n_{\mu\nu}(x) \frac{\chi^n(y)}{\sqrt{b_0}} \qquad \Longrightarrow \qquad \mathcal{L}_{\rm int} = -\frac{1}{\widehat{\Lambda}_W} \sum_{n \neq 0} h^n_{\mu\nu} T^{\mu\nu} - \frac{\phi_0}{\Lambda_\phi} T^\mu_\mu$$

for

$$\widehat{\Lambda}_W \simeq \sqrt{2} m_{Pl} \Omega_0, \;\; \Lambda_\phi = \sqrt{3} \widehat{\Lambda}_W, \;\; \Omega_0 = e^{-m_0 b_0/2} \;\; \text{and} \;\; \phi_0(x) \equiv \sqrt{6} m_{Pl} e^{-m_0 (b_0 + b(x))/2}$$

$$S_\xi = \xi \int d^4x \sqrt{g_{\rm vis}} R(g_{\rm vis}) H^\dagger H,$$

where $R(g_{\rm vis})$ is the Ricci scalar for the metric induced on the visible brane.

$$\mathcal{L}_{\rm kin} = -\frac{1}{2}(1+6\gamma^2\xi)\phi_0 \Box \phi_0 - \frac{1}{2}\phi_0 m_{\phi_0}^2 \phi_0 - \frac{1}{2} h_0 (\Box + m_{h_0}^2) h_0 - 6\gamma\xi\phi_0 \Box h_0,$$

where $\gamma \equiv v_0/\Lambda_\phi$

$$\tan 2\theta \equiv 12\gamma\xi Z \frac{m_{h_0}^2}{m_{\phi_0}^2 - m_{h_0}^2 (Z^2 - 36\xi^2\gamma^2)} \quad \text{for} \quad Z^2 \equiv 1 + 6\xi\gamma^2(1-6\xi)$$

Canonically normalized states that diagonalize the kinetic energy are h and ϕ:

$$\begin{aligned} h_0 &= \left(\cos\theta - \frac{6\xi\gamma}{Z}\sin\theta\right) h + \left(\sin\theta + \frac{6\xi\gamma}{Z}\cos\theta\right)\phi \\ \phi_0 &= -\cos\theta\frac{\phi}{Z} + \sin\theta\frac{h}{Z} \end{aligned}$$

Remarks:

- The RS model provides a simple solution to the hierarchy problem if the Higgs is placed on the TeV brane at $y = 1/2$ by virtue of the fact that the 4D electro-weak scale v_0 is given in terms of the $\mathcal{O}(m_{Pl})$ 5D Higgs vev, $\widehat{v}$, by:

$$v_0 = \Omega_0 \widehat{v} = e^{-\frac{1}{2} m_0 b_0} \widehat{v} \sim 1 \text{ TeV} \qquad \text{for} \qquad \frac{1}{2} m_0 b_0 \sim 35$$

  As a result, to solve the hierarchy problem, $\Lambda_\phi = \sqrt{6} m_{Pl} \Omega_0$ should be of order $1 - 10$ TeV, but not much higher

- non-unitarity

$$g^2_{ZZh} + g^2_{ZZ\phi} = 1 + \frac{\gamma^2 (1 - 6\xi)^2}{Z^2}$$

Higher-dimensional operators in the 5D effective field theory are suppressed only by TeV^{-1} and then FCNC processes and PEW observable corrections are predicted to be much too large.

$$\Downarrow$$

It is therefore now regarded as necessary to allow all the SM fields (except the Higgs) to propagate in the extra dimension. The SM particles are then the zero-modes of the 5D fields and the profile of a SM fermion in the extra dimension can be adjusted using a mass parameter.

For example, for the W we have (before mixing)

$$\mathcal{L} \ni h_0 \frac{2m_W^2}{v} W_\mu^\dagger W^\mu - \phi_0 \frac{2m_W^2}{\Lambda_\phi} \left[W_\mu^\dagger W^\mu \left(1 - \kappa_W\right) + W_{\mu\nu}^\dagger W^{\mu\nu} \frac{1}{4m_W^2 (\frac{1}{2} m_0 b_0)} \right]$$

where $\kappa_V = \left(\frac{3m_V^2 (\frac{1}{2} m_0 b_0)}{\Lambda_\phi^2 (m_0/m_{Pl})^2} \right)$ for $V = W, Z$.

After mixing, this becomes, for example for the h interaction

$$\mathcal{L} \ni h \frac{2m_W^2}{v} \left[g_h^W W_\mu^\dagger W^\mu + g_h^r \frac{1}{4m_W^2 (\frac{1}{2} m_0 b_0)} W_{\mu\nu}^\dagger W^{\mu\nu} \right]$$

with a similar result for the ϕ.

$$m_1^g = \frac{x_1^g}{\sqrt{6}} \frac{m_0}{m_{Pl}} \Lambda_\phi \qquad \text{for} \qquad x_1^g = 2.45$$

Scenarios:

- A strong lower bound on the masses of the first excitations of the gauge bosons applies (CMS): $m_1^g \geq 1.5$ TeV (K. Agashe *et al.*, Phys. Rev. D **77**, 015003 (2008)) When $m_1^g \geq 1.5$ TeV then

$$\Lambda_\phi \lesssim 10 \text{ TeV} \Rightarrow \frac{m_0}{m_{Pl}} \gtrsim 0.15$$

  Thus, a significant lower bound on m_1^g implies that only relatively large values for m_0/m_{Pl} are allowed. For phenomenology we adopt (fixed m_1^g):

$$\Lambda_\phi = m_1^g \frac{\sqrt{6}}{x_1^g} \left(\frac{m_0}{m_{Pl}} \right)^{-1}$$

- Fermionic profiles (flat for light quarks) are such that the bounds on the gauge boson excitations are very weak. Then no substantial experimental limits on m_1^g could be obtained (fixed Λ_ϕ adopted).

$$R_h(X) \equiv \frac{\Gamma_h(gg)BR(h \to X)}{\Gamma_{h_{SM}}(gg)BR(h_{SM} \to X)}\,, \quad R_\phi(X) \equiv \frac{\Gamma_\phi(gg)BR(\phi \to X)}{\Gamma_{h_{SM}}(gg)BR(h_{SM} \to X)}\,,$$

$$X = \gamma\gamma, ZZ, b\bar{b}$$

Signals

- Signal at only 125 GeV
- Signal (h or ϕ) at 125 GeV and high mass $m_\phi \gtrsim 500$ GeV

Signal at only 125 GeV ($m_1^g = 1.5$ TeV)

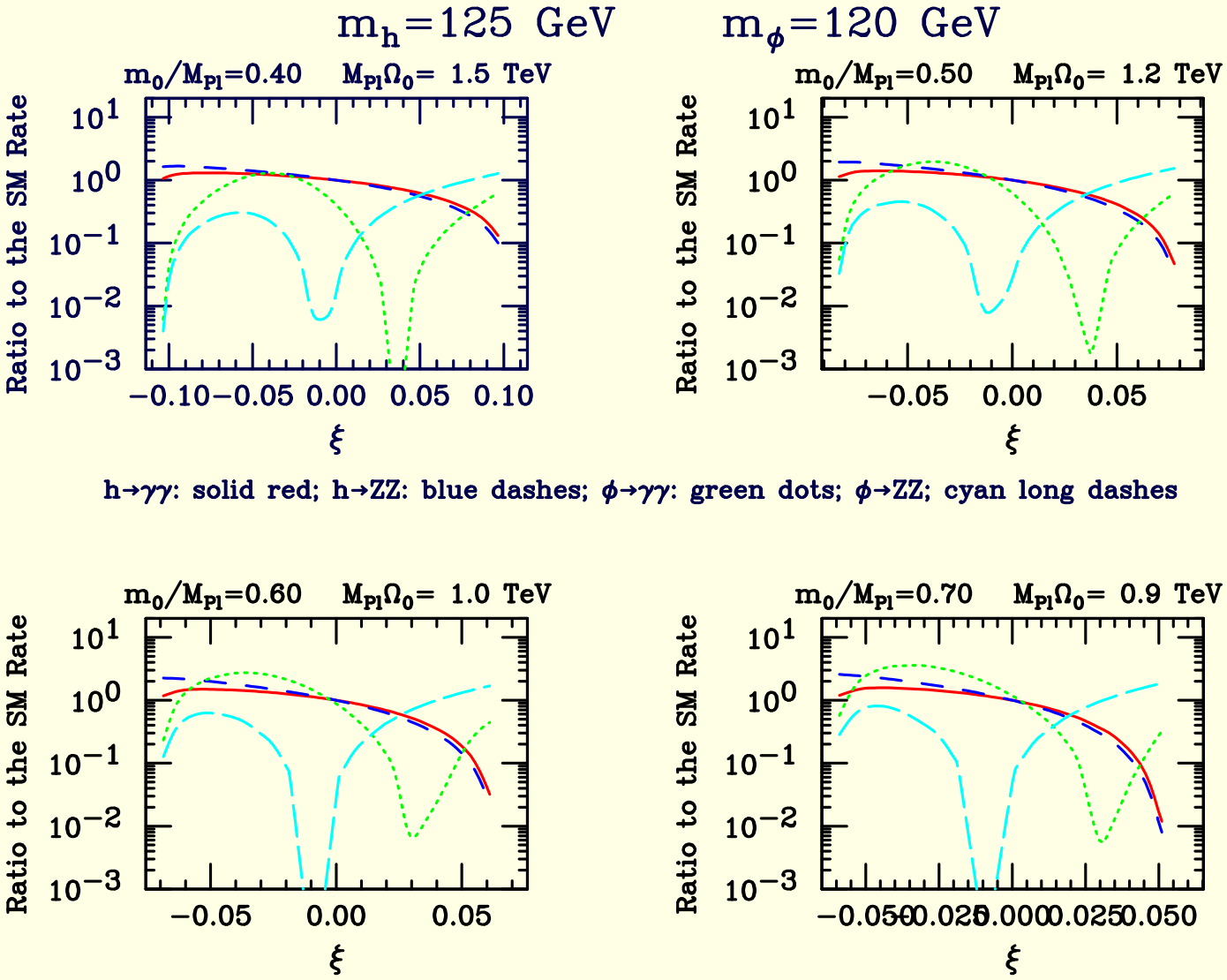

Figure 3: For $m_h = 125$ GeV and $m_\phi = 120$ GeV, we plot $R_h(X)$ and $R_\phi(X)$ for $X = \gamma\gamma$ and $X = ZZ$ (equivalent to $X = 4\ell$) as a function of ξ, assuming $m_1^g = 1.5$ TeV.

Signal (h or ϕ) at 125 GeV and high mass ($m_1^g = 1.5$ TeV)

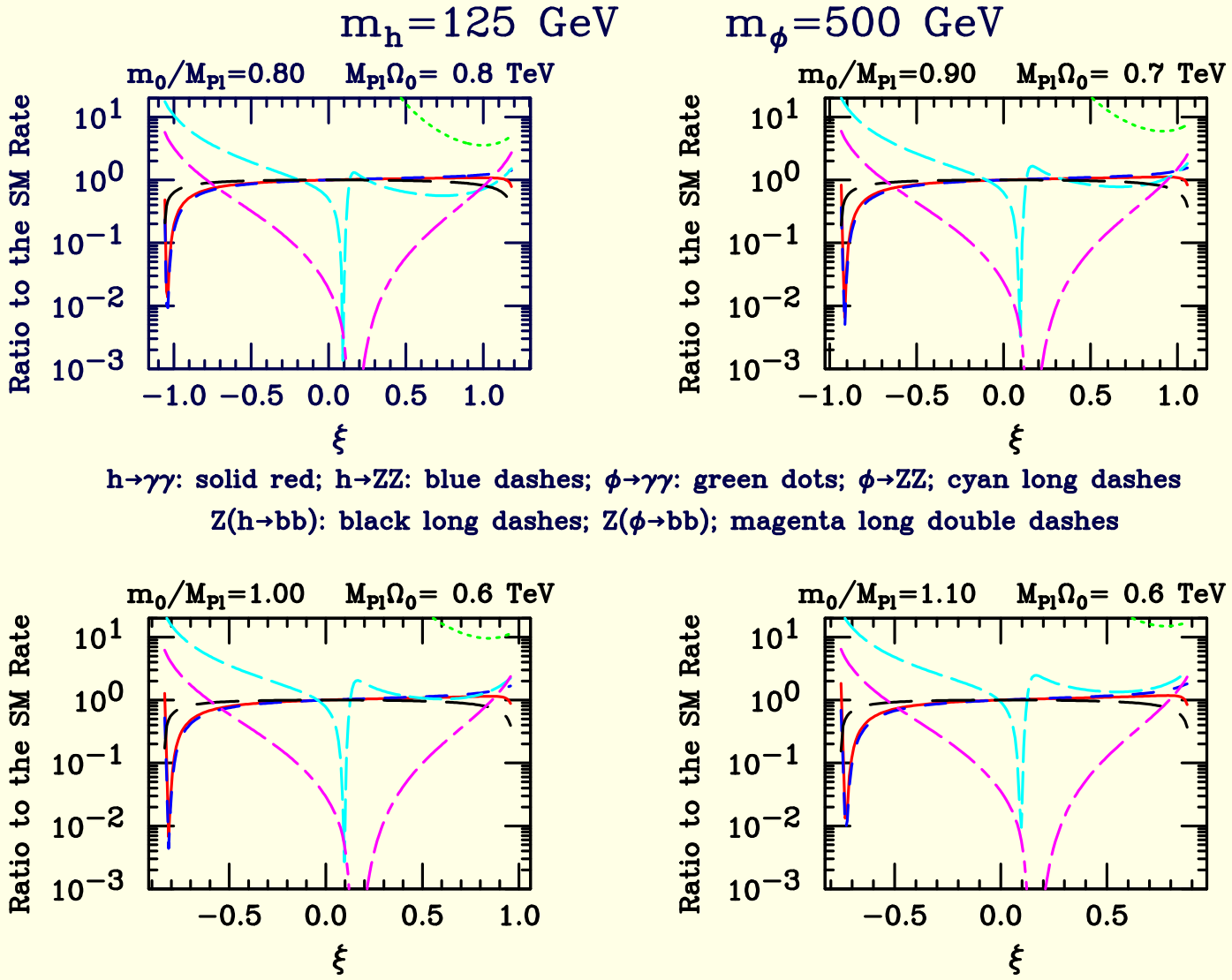

Figure 4: For $m_h = 125$ GeV and $m_\phi = 500$ GeV, we plot $R_h(X)$ and $R_\phi(X)$ for $X = \gamma\gamma$ and $X = ZZ$ (equivalent to $X = 4l$) as a function of ξ, assuming $m_1^g = 1.5$ TeV. Also shown are the similarly defined ratios for $Z + h$ production with $h \to b\bar{b}$ and $Z + \phi$ production with $\phi \to b\bar{b}$.

Signal at only 125 GeV (fixed $\Lambda_\phi = 1$ TeV)

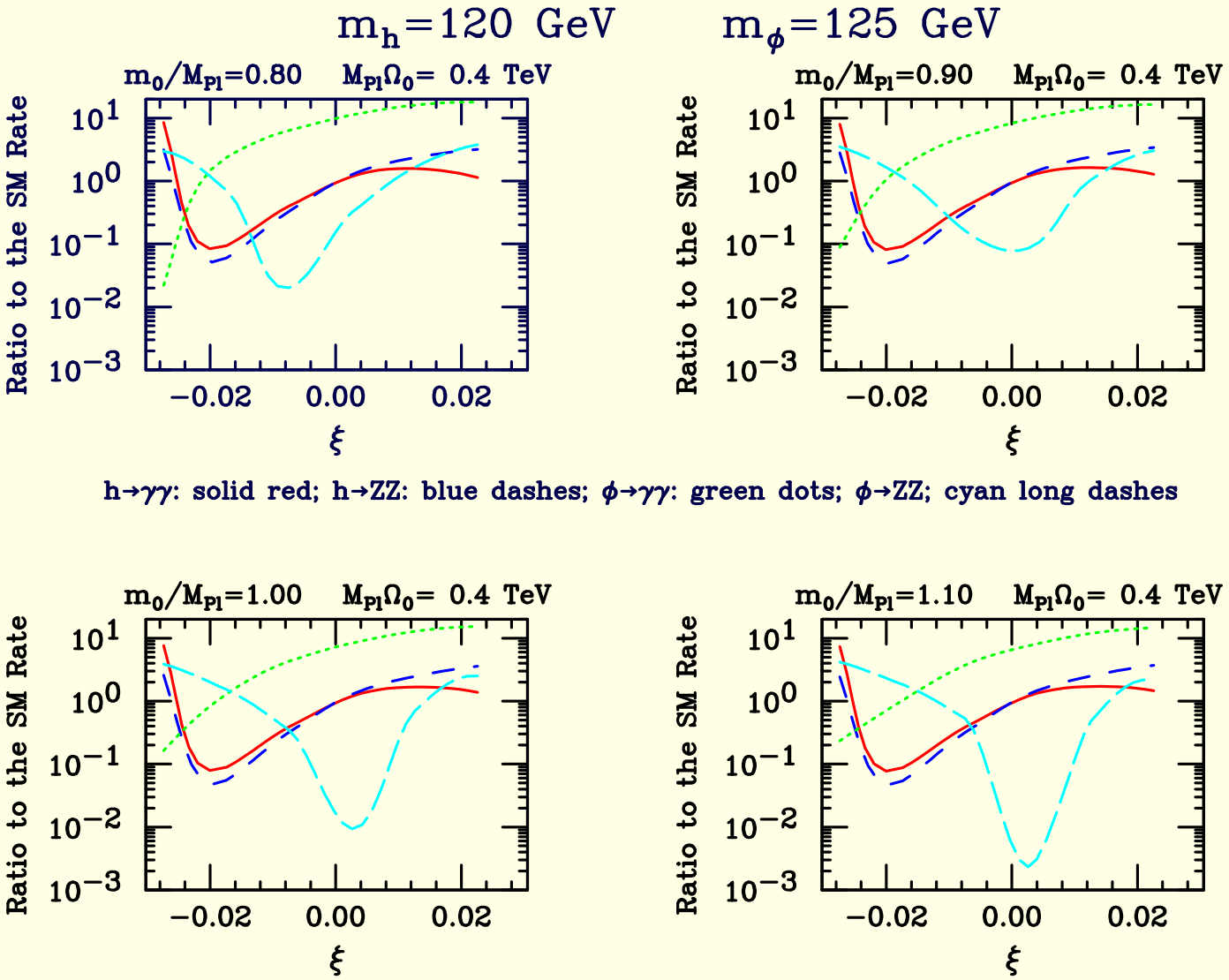

Figure 5: For $m_h = 120$ GeV and $m_\phi = 125$ GeV, we plot $R_h(X)$ and $R_\phi(X)$ for $X = \gamma\gamma$ and $X = ZZ$ (equivalent to $X = 4\ell$) as a function of ξ taking Λ_ϕ fixed at 1 TeV.

Conclusions on the Gravity-Higgs mixing setup:

- Fixed $m_1^g = 1.5$ TeV scenario:
  - Signal at only 125 GeV: consistent parameters could be found for $m_h = 125$ GeV and $m_\phi = 120$ GeV: e.g. $m_0/m_{Pl} = 0.4$ and $\xi \sim -0.09$.
  - Signal (h or ϕ) at 125 GeV and high mass: too large $|\xi|$ is needed (difficulties with precision electroweak constraints).

- Fixed $\Lambda_\phi = 1$ TeV scenario:
  - Signal at only 125 GeV: consistent parameters could be found for $m_h = 120$ GeV and $m_\phi = 125$ GeV: e.g. $m_0/m_{Pl} = 1$ and $\xi \sim -0.016$.
  - Signal (h or ϕ) at 125 GeV and high mass: no consistent and interesting solution.

Second Higgs doublet

♠ Type I and II models

$$V(\Phi_1,\Phi_2) = m_{11}^2\Phi_1^\dagger\Phi_1 + m_{22}^2\Phi_2^\dagger\Phi_2 - \left[m_{12}^2\Phi_1^\dagger\Phi_2 + \text{h.c.}\right]$$
$$+ \frac{\lambda_1}{2}\left(\Phi_1^\dagger\Phi_1\right)^2 + \frac{\lambda_2}{2}\left(\Phi_2^\dagger\Phi_2\right)^2 + \lambda_3\left(\Phi_1^\dagger\Phi_1\right)\left(\Phi_2^\dagger\Phi_2\right) + \lambda_4\left(\Phi_1^\dagger\Phi_2\right)\left(\Phi_2^\dagger\Phi_1\right)$$
$$+ \left\{\frac{\lambda_5}{2}\left(\Phi_1^\dagger\Phi_2\right)^2 + \left[\lambda_6\left(\Phi_1^\dagger\Phi_1\right) + \lambda_7\left(\Phi_2^\dagger\Phi_2\right)\right]\left(\Phi_1^\dagger\Phi_2\right) + \text{h.c.}\right\}.$$

$$\langle\Phi_1\rangle = \frac{v}{\sqrt{2}}\begin{pmatrix}0\\ \cos\beta\end{pmatrix} \qquad \langle\Phi_2\rangle = \frac{v}{\sqrt{2}}\begin{pmatrix}0\\ e^{i\xi}\sin\beta\end{pmatrix},$$

where $v = (\sqrt{2}G_F)^{-1/2} \approx 246$ GeV and $\xi = 0$.

$$\Phi_a = \begin{pmatrix}\phi_a\\ (v_a + \rho_a + i\eta_a)/\sqrt{2}\end{pmatrix} \qquad a = 1,2$$

with $v_1 = v\cos\beta$ and $v_2 = v\sin\beta$.

The neutral Goldstone boson

$$G^0 = \eta_1 \cos\beta + \eta_2 \sin\beta$$

The physical pseudoscalar

$$A = -\eta_1 \sin\beta + \eta_2 \cos\beta$$

The physical scalars are:

$$h = -\rho_1 \sin\alpha + \rho_2 \cos\alpha, \quad H = \rho_1 \cos\alpha + \rho_2 \sin\alpha$$

The LHC signal normalized to the SM prediction

$$R_{gg}^{h_i}(X) \equiv \frac{\Gamma(gg \to h_i)\ BR(h_i \to X)}{\Gamma(gg \to h_{SM})\ BR(h_{SM} \to X)}$$

for $X = \gamma\gamma, ZZ, b\bar{b}$ and $h_i = h, H, \cdots$

Earlier works:

- P. M. Ferreira, R. Santos, M. Sher and J. P. Silva, "Could the LHC two-photon signal correspond to the heavier scalar in two-Higgs-doublet models?," Phys. Rev. D **85**, 035020 (2012) [arXiv:1201.0019 [hep-ph]].

- P. M. Ferreira, R. Santos, M. Sher and J. P. Silva, "Implications of the LHC two-photon signal for two-Higgs-doublet models," Phys. Rev. D **85**, 077703 (2012) [arXiv:1112.3277 [hep-ph]].

- ???

$$\mathcal{L}_Y^{(q)} = \bar{Q}_L \tilde{\Gamma}_1 u_R \tilde{\Phi}_1 + \bar{Q}_L \Gamma_1 d_R \Phi_1 + \bar{Q}_L \tilde{\Gamma}_2 u_R \tilde{\Phi}_2 + \bar{Q}_L \Gamma_2 d_R \Phi_2 + \text{H.c.}$$

then

$$M_u = -\tilde{\Gamma}_1 \left\langle \tilde{\Phi}_1 \right\rangle - \tilde{\Gamma}_2 \left\langle \tilde{\Phi}_2 \right\rangle \qquad M_d = -\Gamma_1 \langle \Phi_1 \rangle - \Gamma_2 \langle \Phi_2 \rangle$$

Natural Flavour Conservation:

- Type I model, $\mathbb{Z}_2$ softly broken (by $m_{12}^2 \neq 0$): $\Phi_1 \to -\Phi_1 \Rightarrow \lambda_6 = \lambda_7 = 0$
- Type II model, $\mathbb{Z}_2$ softly broken (by $m_{12}^2 \neq 0$): $\Phi_1 \to -\Phi_1$ and $d_R \to -d_R \Rightarrow \lambda_6 = \lambda_7 = 0$

Table 1: Fermionic coupling patterns for Type I and Type II two-Higgs-doublet models.

	Type I			Type II		
Higgs	up quarks	down quarks	leptons	up quarks	down quarks	leptons
h	$\cos\alpha/\sin\beta$	$\cos\alpha/\sin\beta$	$\cos\alpha/\sin\beta$	$\cos\alpha/\sin\beta$	$-\sin\alpha/\cos\beta$	$-\sin\alpha/\cos\beta$
H	$\sin\alpha/\sin\beta$	$\sin\alpha/\sin\beta$	$\sin\alpha/\sin\beta$	$\sin\alpha/\sin\beta$	$\cos\alpha/\cos\beta$	$\cos\alpha/\cos\beta$
A	$\cot\beta$	$-\cot\beta$	$-\cot\beta$	$\cot\beta$	$\tan\beta$	$\tan\beta$

Strategy: scanning and experimental constraints

The input parameters:

- the physical Higgs boson masses $(m_H, m_h, m_A, m_{H^\pm})$,
- the vacuum expectation value ratio $(\tan\beta)$,
- the CP-even Higgs mixing angle (α),
- m_{12}^2.

With the above inputs, $\lambda_{1,2,3,4,5}$ as well as m_{11}^2 and m_{22}^2 are determined (the latter two via the minimization conditions).

We adopted (and modified) the 2HDMC code for branching ratio calculations (D. Eriksson, J. Rathsman and O. Stal, Comput. Phys. Commun. **181**, 189 (2010) [arXiv:0902.0851]).

Scanning scenarios

I. $m_h = 125$ GeV

II. $m_H = 125$ GeV

III. $m_h = m_H = 125$ GeV

IV. $m_h = m_A = 125$ GeV

V. $m_H = m_A = 125$ GeV

	scenario I	scenario II	scenario III	scenario IV	scenario V
m_h [GeV]	125	{10,. . . , 124.9}	125	125	{10,. . . , 124.9}
m_H [GeV]	125+{0.1,. . . ,1000}	125	125.1	125+{0.1,. . . ,1000}	125
m_A [GeV]	{10,. . . ,1000}	{10,. . . ,1000}	{10,. . . ,1000}	125.1	125.1
$m_{H^\pm}$ [GeV]	1500 ($\tan\beta$=0.5); 800 ($\tan\beta$=1); 350 ($\tan\beta$=2); 90,150,250,350 for Type I 600 ($\tan\beta$=0.5); 500 ($\tan\beta$=1); 340 ($\tan\beta$=2); 320 for Type II				
$\tan\beta$	{0.5, . . . , 20}				
$\sin\alpha$	{-1, . . . ,1}				
m_{12}^2 [GeV^2]	$\{-1000^2,\ldots,1000^2\}$				

Experimental constraints

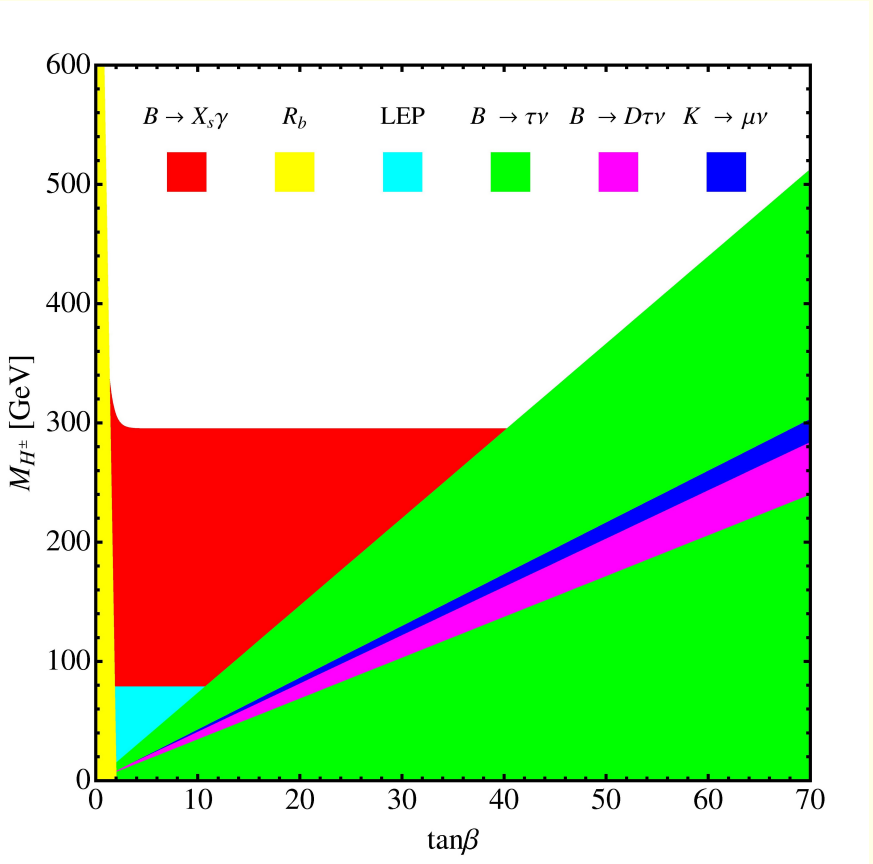

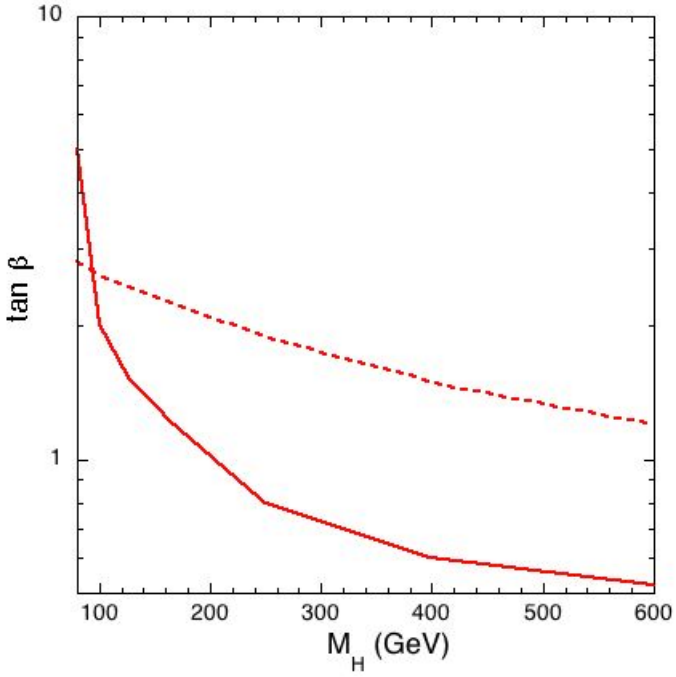

Figure 6: 1) Bounds in the $m_{H^\pm} - \tan\beta$ plane from various B-physics constraints for the type II model (U. Haisch, arXiv:0805.2141). 2) Lower bounds on $\tan\beta$ in the type I model as a function of the charged-Higgs mass $m_{H^\pm}$. The solid line is the bound is from $Z \to b\bar{b}$, ϵ_K and Δm_{B_s} (M. Jung, A. Pich and P. Tuzon, JHEP **1011**, 003 (2010), [arXiv:1006.0470]). The dashed line comes from $B \to \gamma X_s$ (F. Mahmoudi and O. Stal, Phys. Rev. D **81**, 035016 (2010) [arXiv:0907.1791]; R. S. Gupta and J. D. Wells, Phys. Rev. D **81**, 055012 (2010) [arXiv:0912.0267]).

Theoretical constraints:

- Perturbative unitarity: $|L_i| \leq 8\pi$
- Perturbativity: $|C_{H_i H_j H_k H_l}| \leq 4\pi$
- Vacuum stability: $\lambda_{1,2} > 0, \;\; \lambda_3 > -\sqrt{\lambda_1 \lambda_2}, \;\; \lambda_3 + \lambda_4 - |\lambda_5| > -\sqrt{\lambda_1 \lambda_2}$

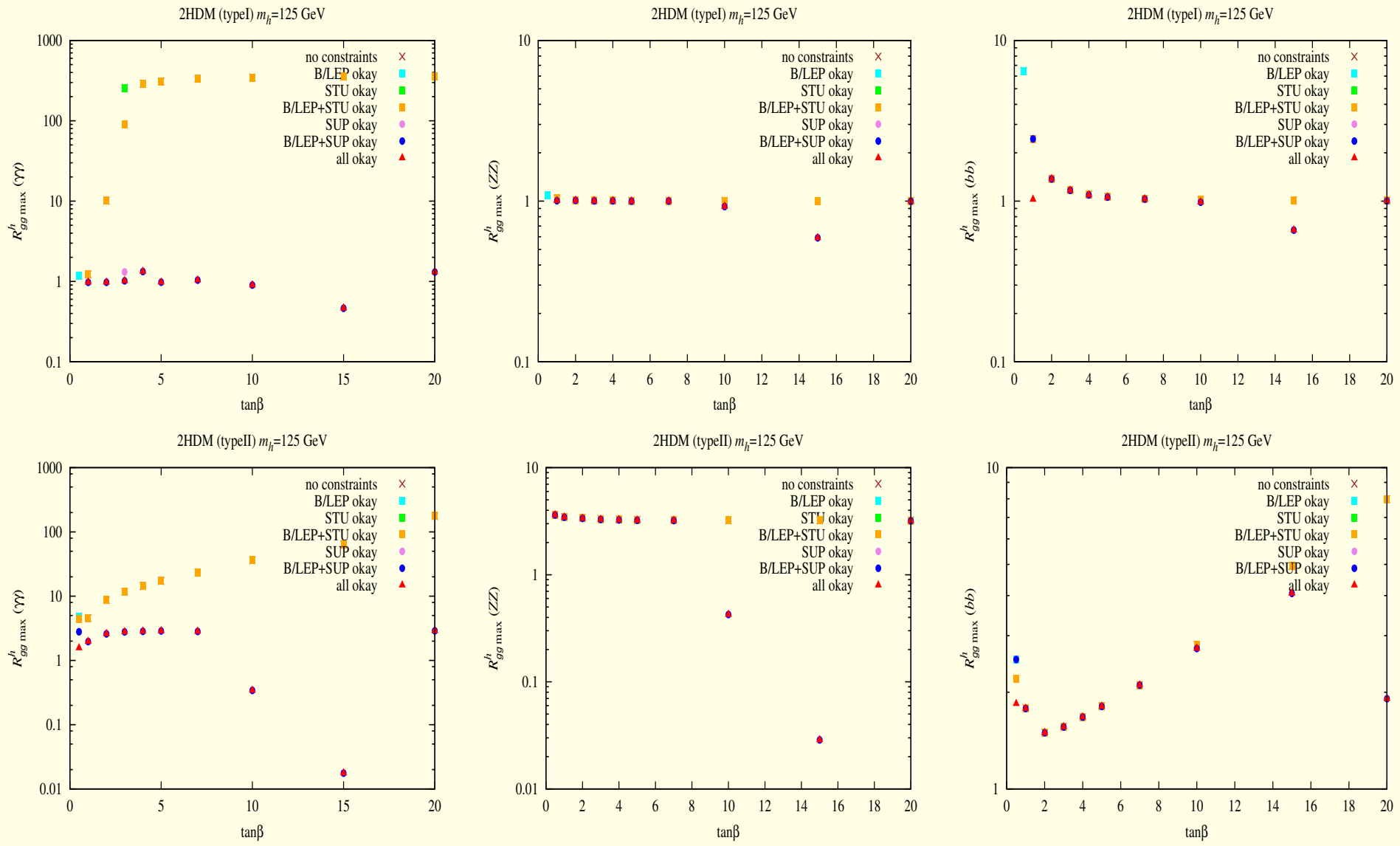

Figure 7: $R^h_{gg}(\gamma\gamma)$ maximum values and corresponding $R^h_{gg}(ZZ)$ and $R^h_{gg}(b\bar{b})$ as functions of $\tan\beta$ after imposing various constraints — see figure legend. Disappearance of a point after imposing a given constraint set means that the point did not satisfy that set of constraints. In a case of boxes and circles, if a given point satisfies subsequent constraints then the resulting color is chosen according to the color ordering shown in the legend.

$\tan\beta$	$R^h_{gg\max}(\gamma\gamma)$	$R^h_{gg}(ZZ)$	$R^h_{gg}(b\bar{b})$	$R^h_{\rm VBF}(\gamma\gamma)$	$R^h_{\rm VBF}(ZZ)$	$R^h_{\rm VBF}(b\bar{b})$	m_H	m_A	$m_{H^\pm}$	m_{12}	$\sin\alpha$	$\mathcal{A}^h_{H^\pm}/\mathcal{A}$	δa_μ
1.0	0.98	1.00	1.02	0.96	0.98	1.00	875	750	800	500	-0.7	-0.01	-2.3
2.0	0.98	0.98	0.92	1.04	1.04	0.98	425	500	350	200	-0.5	-0.01	-1.8
3.0	1.02	0.98	0.92	1.08	1.04	0.98	225	400	150	100	-0.4	0.01	-1.7
4.0	1.33	0.99	1.07	1.24	0.93	0.99	225	200	90	100	-0.1	0.14	-1.7
5.0	0.98	0.98	1.06	0.90	0.91	0.98	225	400	150	100	-0.0	0.01	-1.6
7.0	1.04	0.99	0.98	1.06	1.01	0.99	135	500	90	50	-0.2	0.02	-1.6
10.0	0.90	0.81	0.74	0.99	0.89	0.81	175	500	150	50	-0.5	0.04	-1.5
15.0	0.46	0.59	0.66	0.41	0.53	0.59	225	400	350	50	0.6	-0.11	-1.4
20.0	1.31	1.00	1.00	1.30	0.99	1.00	225	200	90	50	-0.0	0.13	-1.5

Table 1: Table of maximum $R^h_{gg}(\gamma\gamma)$ values for Type I 2HDM with $m_h = 125$ GeV and associated input parameters.

$\tan\beta$	$R^h_{gg\max}(\gamma\gamma)$	$R^h_{gg}(ZZ)$	$R^h_{gg}(b\bar{b})$	$R^h_{\rm VBF}(\gamma\gamma)$	$R^h_{\rm VBF}(ZZ)$	$R^h_{\rm VBF}(b\bar{b})$	m_H	m_A	$m_{H^\pm}$	m_{12}	$\sin\alpha$	$\mathcal{A}^h_{H^\pm}/\mathcal{A}$	δa_μ
0.5	1.56	2.69	1.84	0.52	0.89	0.61	425	500	600	100	-0.7	-0.06	-0.5
1.0	1.97	3.36	0.39	0.65	1.11	0.13	125	500	500	100	-0.2	-0.06	0.7
2.0	2.59	3.36	0.00	1.48	1.92	0.00	225	200	340	100	-0.0	-0.05	1.6
3.0	2.78	3.29	0.00	2.01	2.37	0.00	225	200	320	100	-0.0	-0.05	1.6
4.0	2.84	3.25	0.00	2.24	2.57	0.00	225	200	320	100	-0.0	-0.04	1.6
5.0	2.87	3.23	0.00	2.37	2.66	0.00	225	200	320	100	-0.0	-0.04	1.6
7.0	2.83	3.21	0.00	2.42	2.75	0.00	135	300	320	50	-0.0	-0.05	0.8
10.0	0.34	0.43	1.89	0.22	0.28	1.23	325	200	320	100	0.2	-0.08	3.5
15.0	0.02	0.03	4.06	0.00	0.01	0.87	225	200	320	50	0.6	-0.14	5.3
20.0	2.89	3.19	0.00	2.57	2.83	0.00	225	200	320	50	-0.0	-0.04	2.4

Table 2: Table of maximum $R^h_{gg}(\gamma\gamma)$ values for Type II 2HDM with $m_h = 125$ GeV and associated input parameters.

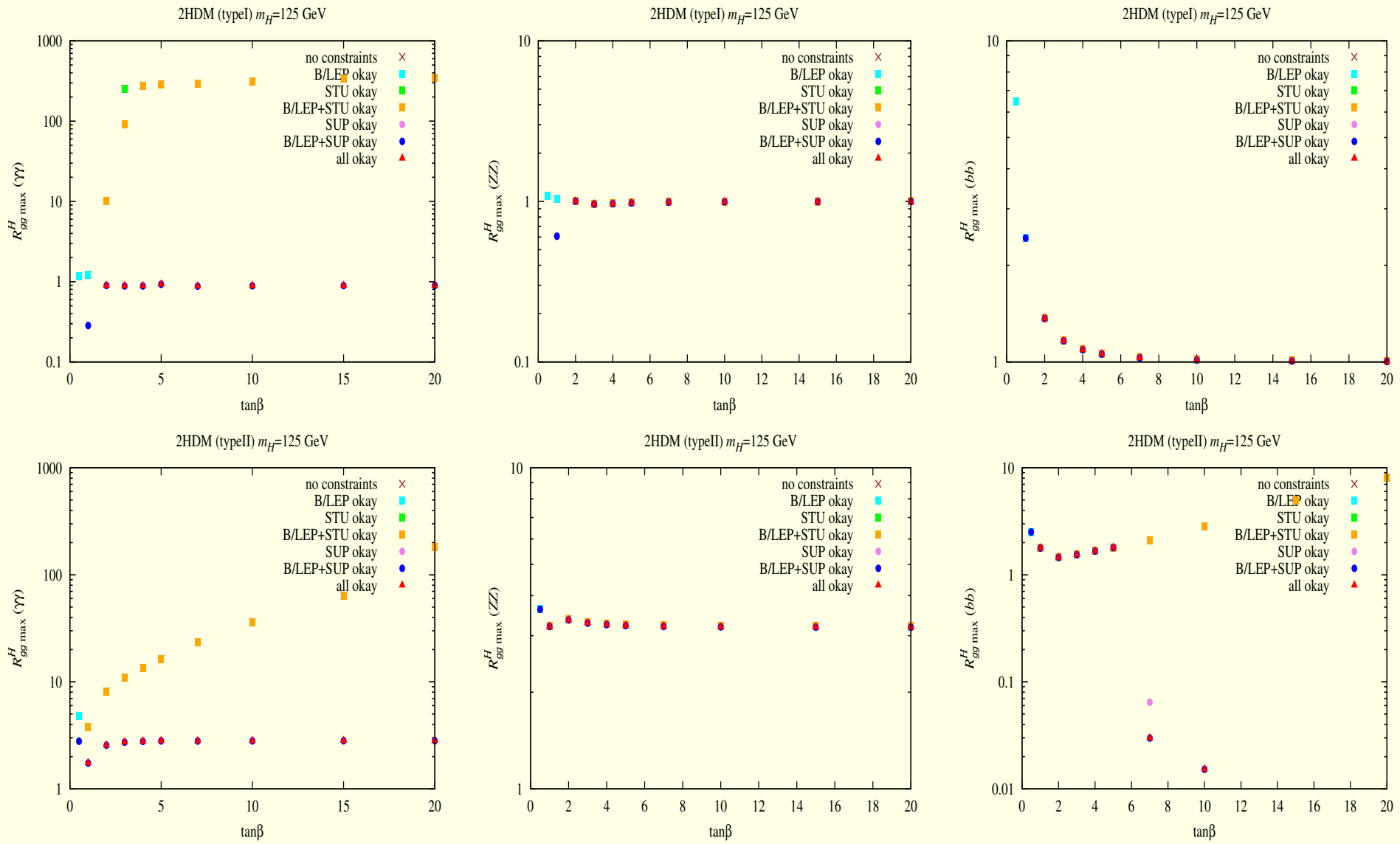

Figure 8: $R^H_{gg}(\gamma\gamma)$ maximum values and corresponding $R^H_{gg}(ZZ)$ and $R^H_{gg}(b\bar{b})$ as functions of $\tan\beta$ after imposing various constraints — see figure legend. Disappearance of a point after imposing a given constraint set means that the point did not satisfy that set of constraints.

$\tan\beta$	$R^H_{gg\max}(\gamma\gamma)$	$R^H_{gg}(ZZ)$	$R^H_{gg}(b\bar{b})$	$R^H_{\rm VBF}(\gamma\gamma)$	$R^H_{\rm VBF}(ZZ)$	$R^H_{\rm VBF}(b\bar{b})$	m_h	m_A	$m_{H^\pm}$	m_{12}	$\sin\alpha$	$\mathcal{A}^H_{H^\pm}/\mathcal{A}$	δa_μ
2.0	0.90	1.00	1.02	0.89	0.99	1.00	125	400	350	50	0.9	-0.05	-2.1
3.0	0.89	0.96	0.88	0.97	1.05	0.96	125	400	350	50	0.9	-0.05	-1.8
4.0	0.89	0.97	1.09	0.79	0.86	0.97	105	500	90	50	1.0	-0.03	-1.7
5.0	0.93	0.98	1.06	0.86	0.90	0.98	125	500	90	50	1.0	-0.01	-1.6
7.0	0.88	0.99	1.03	0.85	0.95	0.99	65	400	350	10	1.0	-0.05	-1.6
10.0	0.89	1.00	1.02	0.87	0.98	1.00	45	400	350	0	1.0	-0.05	-1.6
15.0	0.90	1.00	1.01	0.89	0.99	1.00	5	400	350	0	-1.0	-0.05	-1.6
20.0	0.90	1.00	1.00	0.89	0.99	1.00	25	400	350	0	-1.0	-0.05	-1.5

Table 3: Table of maximum $R^H_{gg}(\gamma\gamma)$ values for Type I 2HDM with $m_H = 125$ GeV and associated input parameters.

$\tan\beta$	$R^H_{gg\max}(\gamma\gamma)$	$R^H_{gg}(ZZ)$	$R^H_{gg}(b\bar{b})$	$R^H_{\rm VBF}(\gamma\gamma)$	$R^H_{\rm VBF}(ZZ)$	$R^H_{\rm VBF}(b\bar{b})$	m_h	m_A	$m_{H^\pm}$	m_{12}	$\sin\alpha$	$\mathcal{A}^H_{H^\pm}/\mathcal{A}$	δa_μ
1.0	1.74	2.39	1.02	0.91	1.24	0.53	105	500	500	100	0.9	-0.06	0.8
2.0	2.56	3.36	0.00	1.46	1.92	0.00	125	300	340	50	1.0	-0.06	1.1
3.0	2.73	3.29	0.00	1.97	2.37	0.00	125	300	320	50	1.0	-0.05	1.0
4.0	2.78	3.25	0.00	2.20	2.57	0.00	125	300	320	50	-1.0	-0.05	1.0
5.0	2.81	3.23	0.00	2.32	2.66	0.00	125	300	320	50	-1.0	-0.05	0.9
7.0	2.80	3.21	0.00	2.40	2.75	0.00	65	300	320	10	-1.0	-0.06	-0.0
10.0	2.81	3.20	0.00	2.46	2.79	0.00	45	300	320	0	-1.0	-0.06	-2.8
15.0	2.82	3.19	0.00	2.49	2.82	0.00	25	300	320	0	-1.0	-0.05	-16.9
20.0	2.82	3.19	0.00	2.50	2.83	0.00	25	300	320	0	-1.0	-0.05	-30.8

Table 4: Table of maximum $R^H_{gg}(\gamma\gamma)$ values for Type II 2HDM with $m_H = 125$ GeV and associated input parameters.

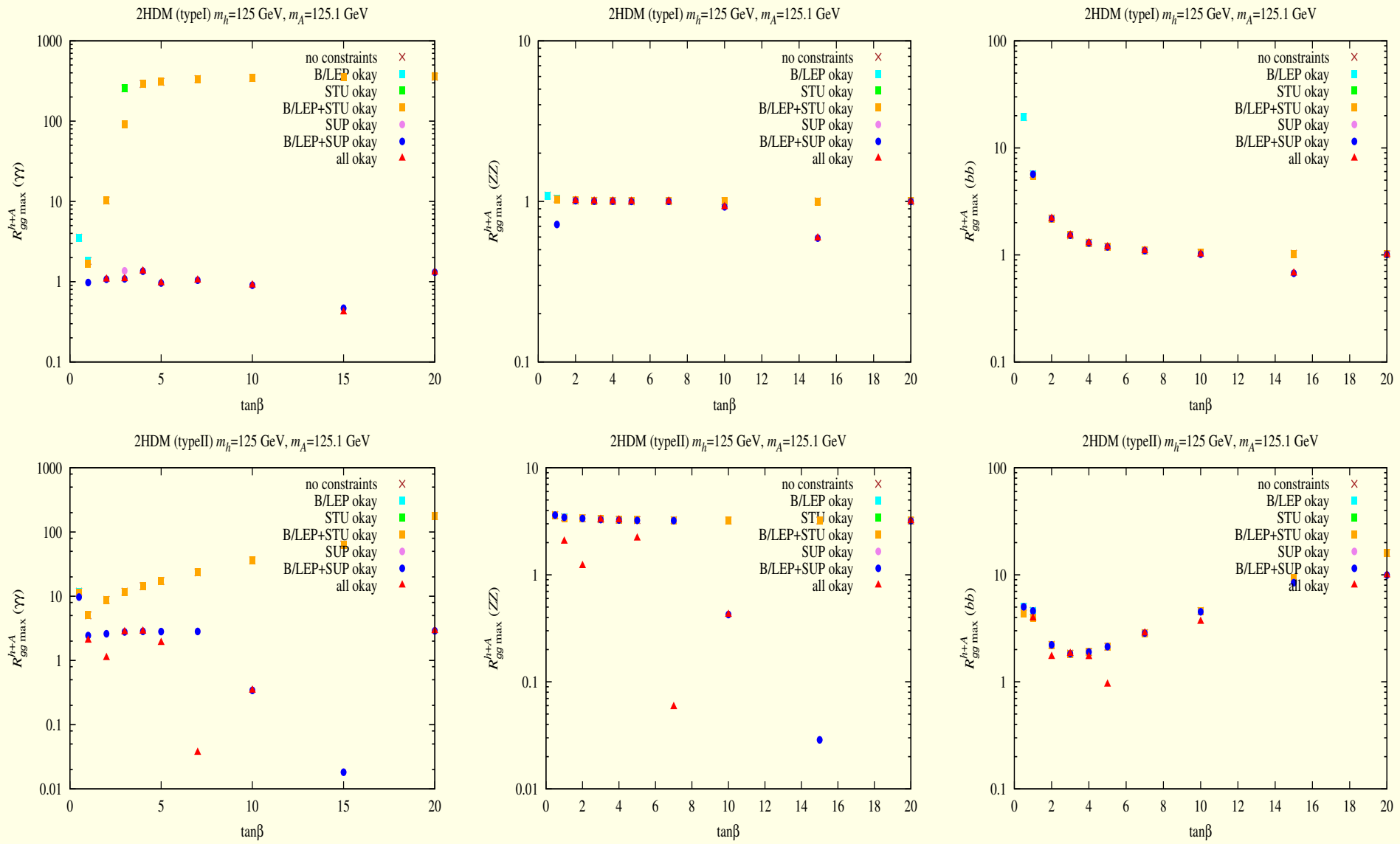

Figure 9: $R_{gg}^{h+A}(\gamma\gamma)$ maximum values when $m_h \simeq m_A = 125$ GeV and corresponding $R_{gg}^{h+A}(ZZ)$ and $R_{gg}^{h+A}(b\bar{b})$ as functions of $\tan\beta$ after imposing various constraints — see figure legend. Disappearance of a point after imposing a given constraint set means that the point did not satisfy that set of constraints.

$\tan\beta$	$R^{h+A}_{gg\max}(\gamma\gamma)$	$R^{h}_{gg}(\gamma\gamma)$	$R^{A}_{gg}(\gamma\gamma)$	$R^{h+A}_{gg}(ZZ)$	$R^{h+A}_{gg}(b\bar{b})$	$R^{h}_{\rm VBF}(\gamma\gamma)$	$R^{h}_{\rm VBF}(ZZ)$	$R^{h}_{\rm VBF}(b\bar{b})$	m_H	$m_{H^\pm}$	m_{12}	$\sin\alpha$	$\mathcal{A}^h_{H^\pm}/\mathcal{A}$	δa_μ
2.0	1.07	0.92	0.15	0.98	1.73	0.98	1.04	0.98	325	250	100	-0.5	-0.04	-2.2
3.0	1.08	1.02	0.07	0.98	1.28	1.08	1.04	0.98	225	150	100	-0.4	0.01	-1.9
4.0	1.35	1.33	0.03	0.99	1.21	1.24	0.93	0.99	225	90	100	-0.1	0.14	-1.8
5.0	0.96	0.95	0.01	1.00	1.07	0.95	1.00	1.00	135	90	50	-0.2	-0.03	-1.7
7.0	1.04	1.04	0.01	0.99	1.00	1.06	1.01	0.99	135	90	50	-0.2	0.02	-1.6
10.0	0.91	0.90	0.01	0.81	0.77	0.99	0.89	0.81	175	150	50	-0.5	0.04	-1.5
15.0	0.42	0.42	0.00	0.59	0.67	0.37	0.53	0.59	225	250	50	0.6	-0.17	-1.4
20.0	1.31	1.31	0.00	1.00	1.00	1.30	0.99	1.00	225	90	50	-0.0	0.13	-1.6

Table 5: Table of maximum $R^{h+A}_{gg}(\gamma\gamma)$ values for Type I 2HDM with $m_h = m_A = 125$ GeV and associated input parameters.

$\tan\beta$	$R^{h+A}_{gg\max}(\gamma\gamma)$	$R^{h}_{gg}(\gamma\gamma)$	$R^{A}_{gg}(\gamma\gamma)$	$R^{h+A}_{gg}(ZZ)$	$R^{h+A}_{gg}(b\bar{b})$	$R^{h}_{\rm VBF}(\gamma\gamma)$	$R^{h}_{\rm VBF}(ZZ)$	$R^{h}_{\rm VBF}(b\bar{b})$	m_H	$m_{H^\pm}$	m_{12}	$\sin\alpha$	$\mathcal{A}^h_{H^\pm}/\mathcal{A}$	δa_μ
1.0	2.05	1.58	0.47	2.05	3.91	0.93	1.22	0.65	525	500	100	-0.5	-0.06	1.3
2.0	1.10	1.09	0.01	1.21	1.69	1.02	1.14	0.91	325	340	100	-0.4	-0.05	1.5
3.0	2.78	2.78	0.00	3.29	0.27	2.01	2.37	0.00	225	320	100	-0.0	-0.05	2.3
4.0	2.84	2.84	0.00	3.25	0.23	2.24	2.57	0.00	225	320	100	-0.0	-0.04	2.3
5.0	1.89	1.89	0.00	2.19	0.95	1.41	1.64	0.47	225	320	100	0.1	-0.05	2.7
7.0	0.04	0.04	0.00	0.06	2.85	0.01	0.02	0.75	325	320	100	0.6	-0.15	5.2
10.0	0.34	0.34	0.00	0.43	3.66	0.22	0.28	1.23	325	320	100	0.2	-0.08	4.7
20.0	2.89	2.89	0.00	3.19	8.03	2.57	2.83	0.00	225	320	50	-0.0	-0.04	5.6

Table 6: Table of maximum $R^{h+A}_{gg}(\gamma\gamma)$ values for Type II 2HDM with $m_h = m_A = 125$ GeV and associated input parameters.

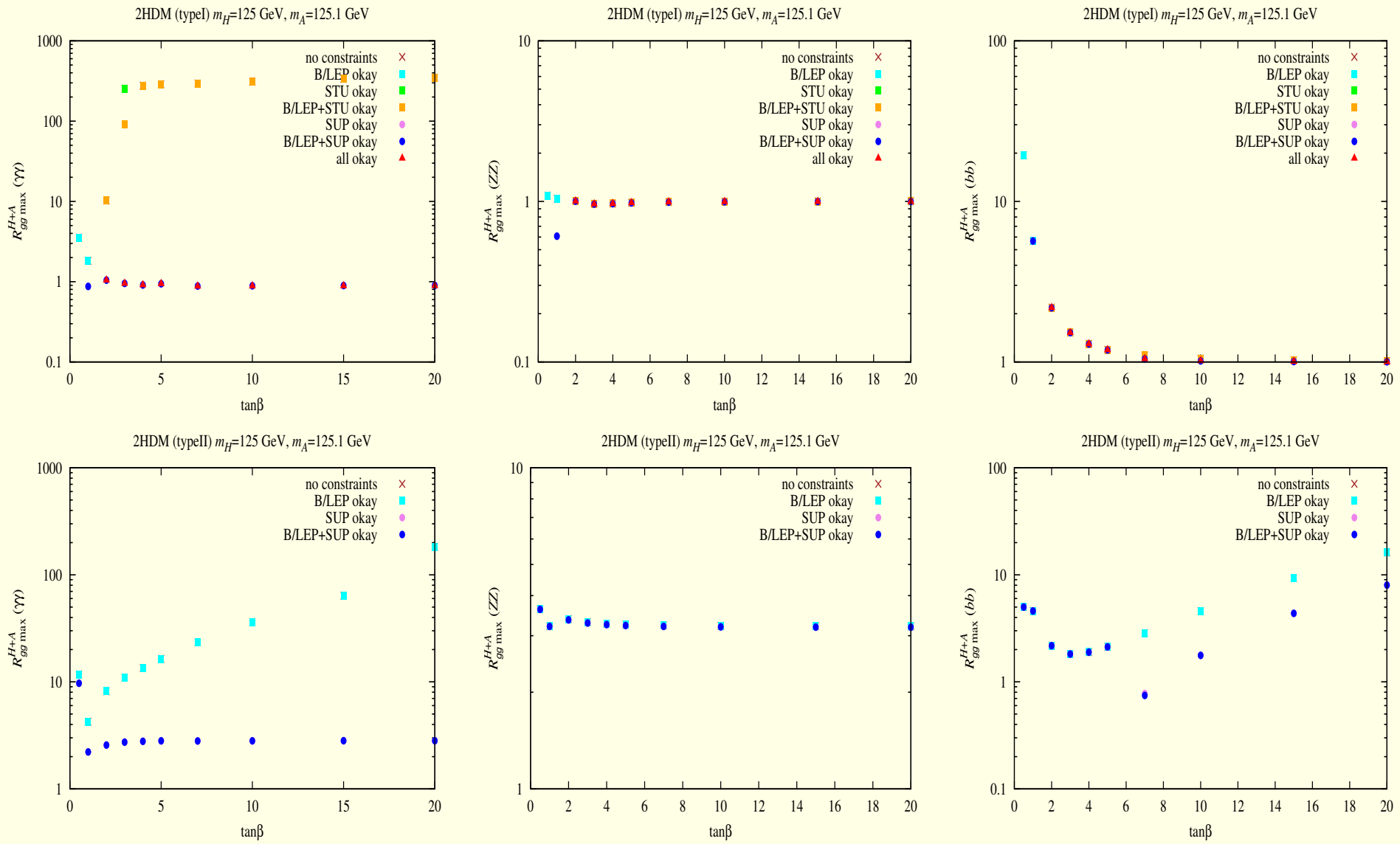

Figure 10: $R_{gg}^{H+A}(\gamma\gamma)$ maximum values when $m_H \simeq m_A = 125$ GeV and corresponding $R_{gg}^{H+A}(ZZ)$ and $R_{gg}^{H+A}(b\bar{b})$ as functions of $\tan\beta$ after imposing various constraints — see figure legend. Disappearance of a point after imposing a given constraint set means that the point did not satisfy that set of constraints.

$\tan\beta$	$R^{H+A}_{gg\max}(\gamma\gamma)$	$R^{H}_{gg}(\gamma\gamma)$	$R^{A}_{gg}(\gamma\gamma)$	$R^{H+A}_{gg}(ZZ)$	$R^{H+A}_{gg}(b\bar{b})$	$R^{H}_{\rm VBF}(\gamma\gamma)$	$R^{H}_{\rm VBF}(ZZ)$	$R^{H}_{\rm VBF}(b\bar{b})$	m_h	$m_{H^\pm}$	m_{12}	$\sin\alpha$	$\mathcal{A}^H_{H^\pm}/\mathcal{A}$	δa_μ
2.0	1.04	0.90	0.15	1.00	1.83	0.88	0.99	1.00	125	250	50	0.9	-0.06	-2.5
3.0	0.95	0.88	0.07	0.96	1.24	0.97	1.05	0.96	125	250	50	0.9	-0.06	-2.0
4.0	0.91	0.89	0.03	0.97	1.23	0.79	0.86	0.97	125	90	50	1.0	-0.03	-1.8
5.0	0.94	0.93	0.01	0.98	1.13	0.86	0.90	0.98	125	90	50	1.0	-0.01	-1.7
7.0	0.88	0.87	0.00	0.99	1.05	0.84	0.95	0.99	65	150	10	1.0	-0.06	-1.6
10.0	0.88	0.88	0.00	1.00	1.02	0.86	0.98	1.00	45	150	0	-1.0	-0.06	-1.6
15.0	0.89	0.89	0.00	1.00	1.01	0.88	0.99	1.00	25	150	0	-1.0	-0.06	-1.6
20.0	0.89	0.89	0.00	1.00	1.00	0.88	0.99	1.00	25	150	0	-1.0	-0.06	-1.6

Table 7: Table of maximum $R^{H+A}_{gg}(\gamma\gamma)$ values for Type I 2HDM with $m_H = m_A = 125$ GeV and associated input parameters.

$\tan\beta$	$R^{h+H}_{gg\max}(\gamma\gamma)$	$R^{h}_{gg}(\gamma\gamma)$	$R^{H}_{gg}(\gamma\gamma)$	$R^{h+H}_{gg}(ZZ)$	$R^{h+H}_{gg}(b\bar{b})$	$R^{h+H}_{\rm VBF}(\gamma\gamma)$	$R^{h+H}_{\rm VBF}(ZZ)$	$R^{h+H}_{\rm VBF}(b\bar{b})$	m_A	$m_{H^\pm}$	m_{12}	$\sin\alpha$	$\mathcal{A}^h_{H^\pm}/\mathcal{A}$	δa_μ
2.0	0.96	0.87	0.10	1.04	1.32	0.76	0.87	1.04	400	350	50	-0.3	-0.06	-2.1
3.0	0.93	0.88	0.05	1.02	1.14	0.83	0.93	1.02	400	350	50	-0.2	-0.05	-1.8
4.0	0.92	0.92	0.00	1.00	1.06	0.90	0.98	1.00	500	90	50	-0.2	-0.04	-1.7
5.0	0.95	0.95	0.00	1.00	1.04	0.92	0.96	1.00	500	90	50	-0.1	-0.02	-1.6

Table 8: Table of maximum $R^{h+H}_{gg}(\gamma\gamma)$ values for Type I 2HDM with $m_h = m_H = 125$ GeV and associated input parameters.

$\tan\beta$	$R^{h+H}_{gg\max}(\gamma\gamma)$	$R^{h}_{gg}(\gamma\gamma)$	$R^{H}_{gg}(\gamma\gamma)$	$R^{h+H}_{gg}(ZZ)$	$R^{h+H}_{gg}(b\bar{b})$	$R^{h+H}_{\rm VBF}(\gamma\gamma)$	$R^{h+H}_{\rm VBF}(ZZ)$	$R^{h+H}_{\rm VBF}(b\bar{b})$	m_A	$m_{H^\pm}$	m_{12}	$\sin\alpha$	$\mathcal{A}^h_{H^\pm}/\mathcal{A}$	δa_μ
1.0	2.08	1.96	0.11	3.09	1.12	0.87	1.25	0.59	500	500	100	-0.3	-0.06	0.7
2.0	2.57	2.56	0.01	3.36	0.09	1.48	1.93	0.30	300	340	50	-0.0	-0.06	1.1
3.0	2.74	2.73	0.00	3.29	0.19	1.98	2.38	0.15	300	320	50	-0.0	-0.05	1.0
4.0	2.79	2.78	0.00	3.25	0.32	2.20	2.57	0.09	300	320	50	-0.0	-0.05	1.0
5.0	2.81	2.81	0.00	3.23	0.48	2.32	2.66	0.06	300	320	50	-0.0	-0.05	0.9

Table 9: Table of maximum $R^{h+H}_{gg}(\gamma\gamma)$ values for Type II 2HDM with $m_h = m_H = 125$ GeV and associated input parameters.

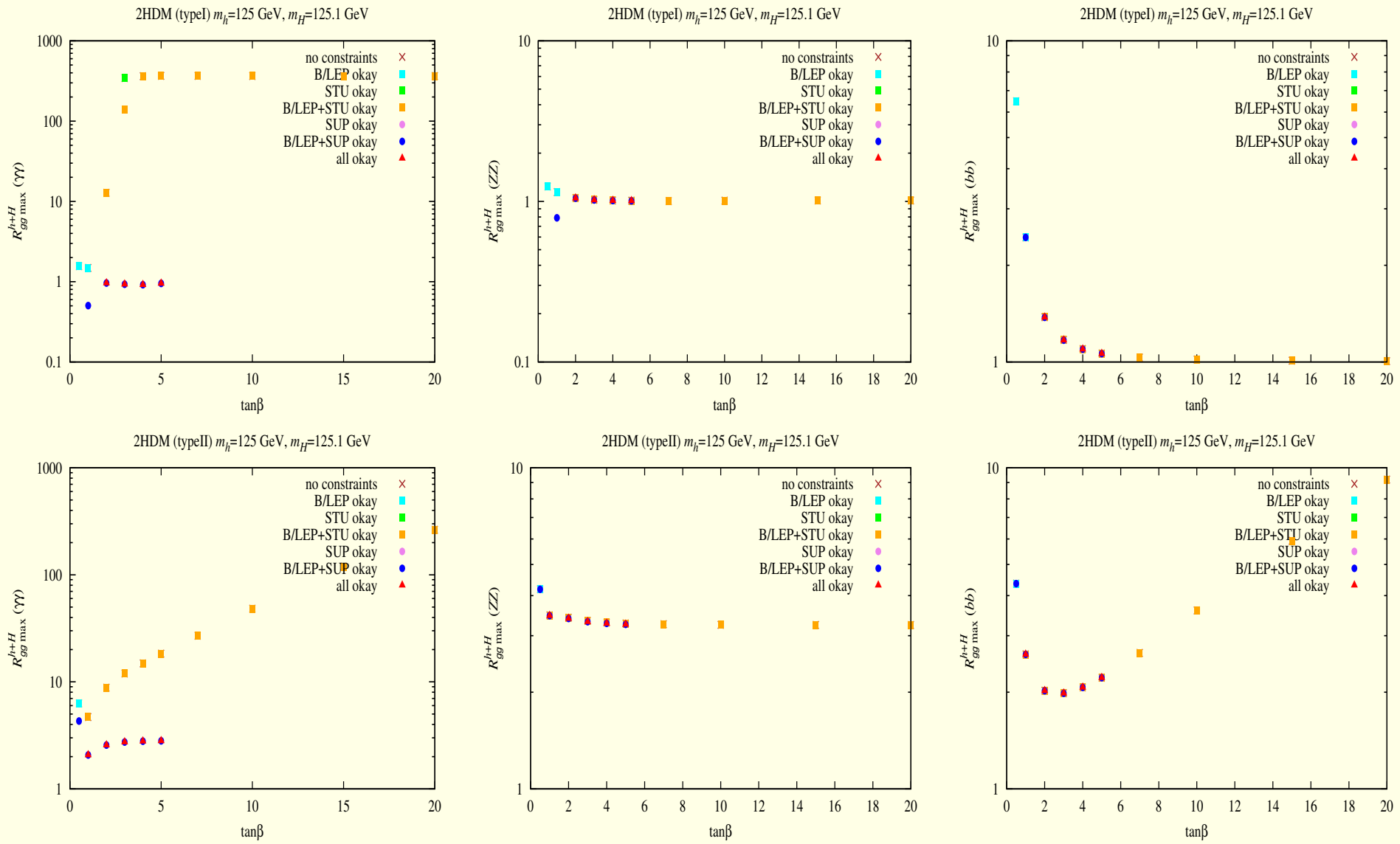

Figure 11: $R^{h+H}_{gg}(\gamma\gamma)$ maximum values when $m_h \simeq m_H = 125$ GeV and corresponding $R^{h+H}_{gg}(ZZ)$ and $R^{h+H}_{gg}(b\bar{b})$ functions of $\tan\beta$ after imposing various constraints — see figure legend. Disappearance of a point after imposing a given constraint set means that the point did not satisfy that set of constraints.

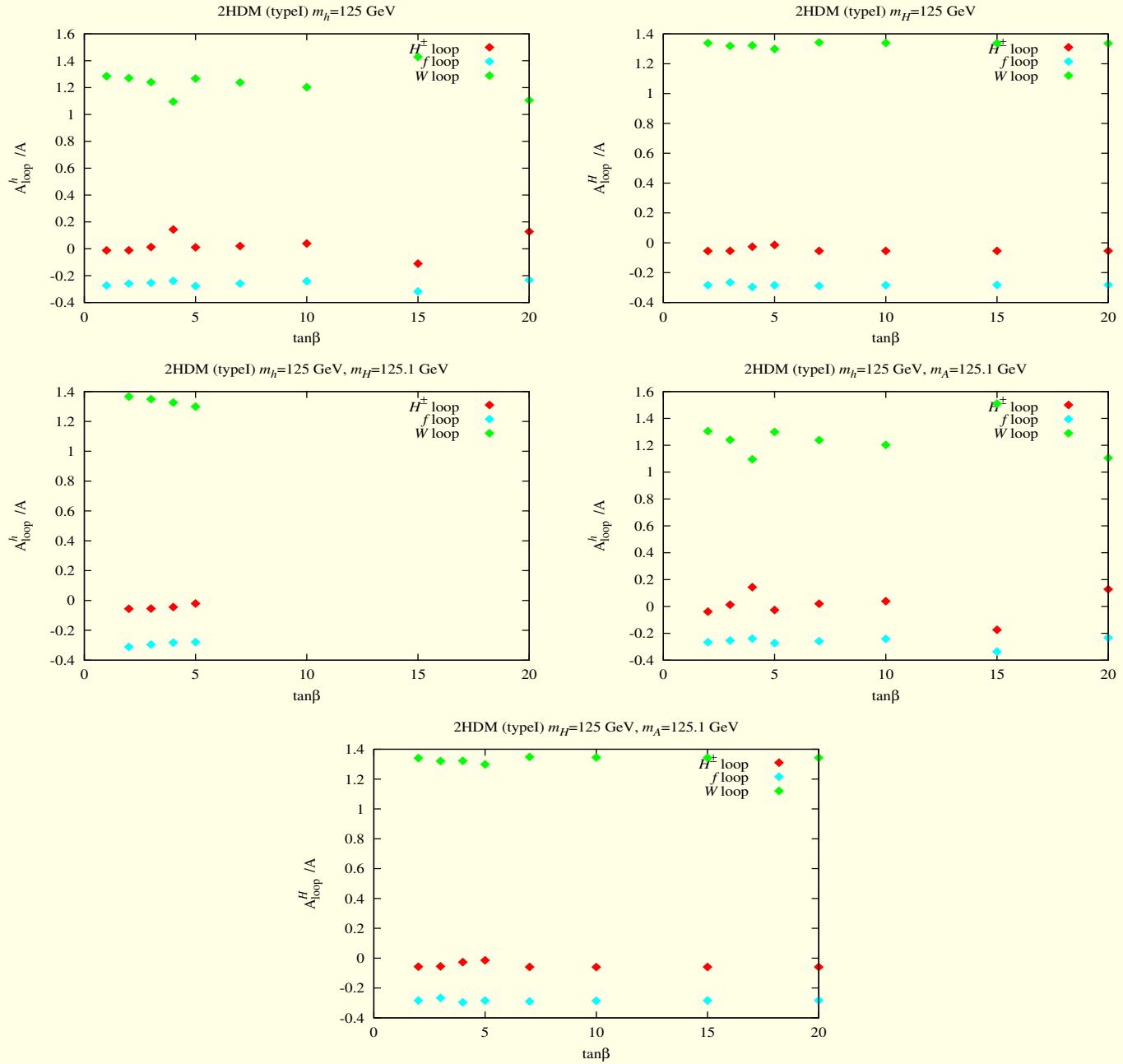

Figure 12: Imaginary part of charged Higgs, fermionic and W contributions to the $\gamma\gamma$ amplitude for the type I model normalized to the imaginary part of the sum of all (fermions, W^+W^-, H^+H^-) contributions as a function of $\tan\beta$ after imposing all constraints. The parameters adopted correspond to maximal $R^{h_i}_{gg}(\gamma\gamma)$ (or an appropriate sum for degenerate cases).

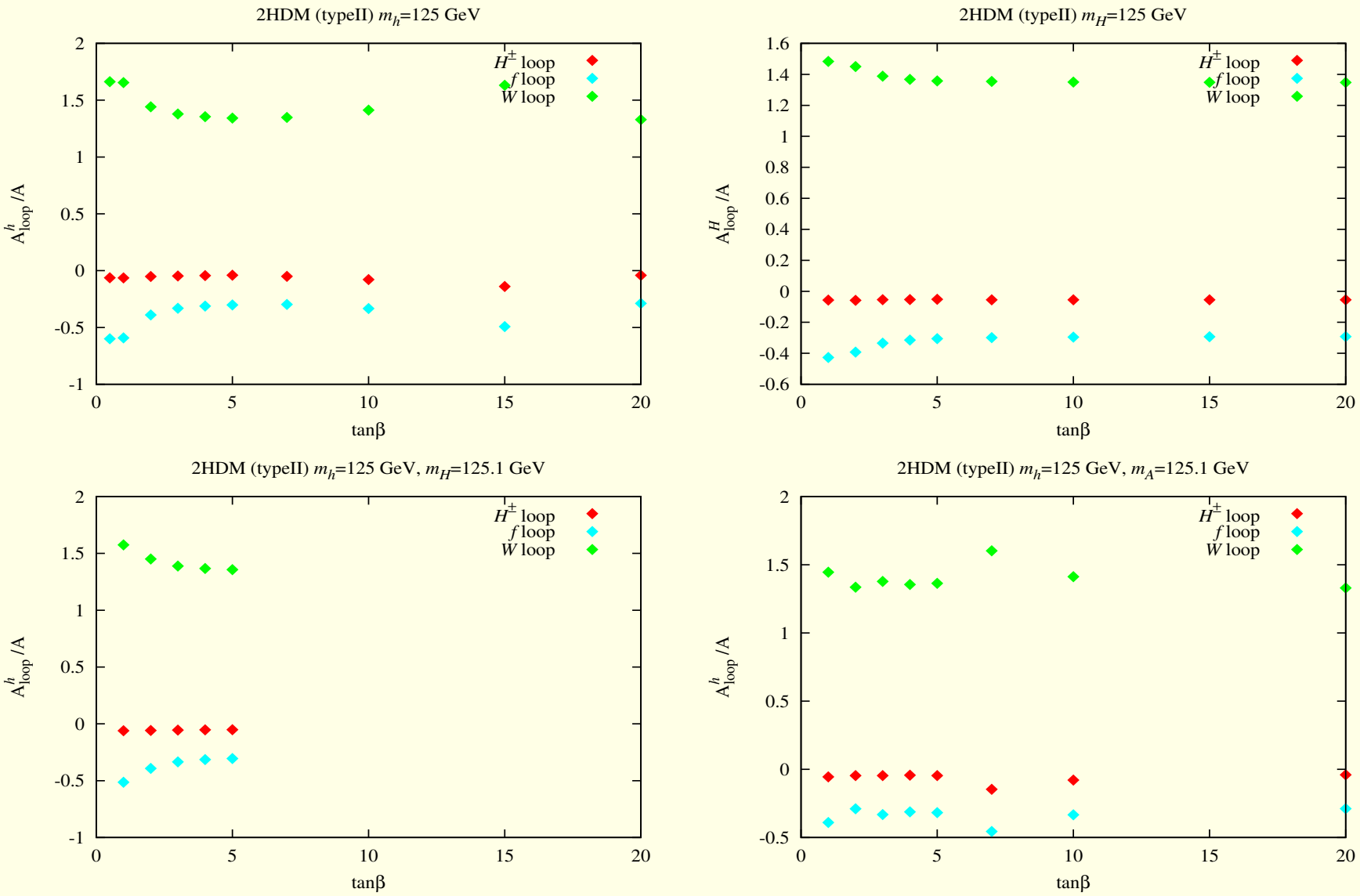

Figure 13: Imaginary part of charged Higgs, fermionic and W contributions to the $\gamma\gamma$ amplitude for the type II model normalized to the imaginary part of the sum of all (fermions, W^+W^-, H^+H^-) contributions as a function of $\tan\beta$ after imposing all constraints. The parameters adopted correspond to maximal $R^{h_i}_{gg}(\gamma\gamma)$ (or an appropriate sum for degenerate cases).

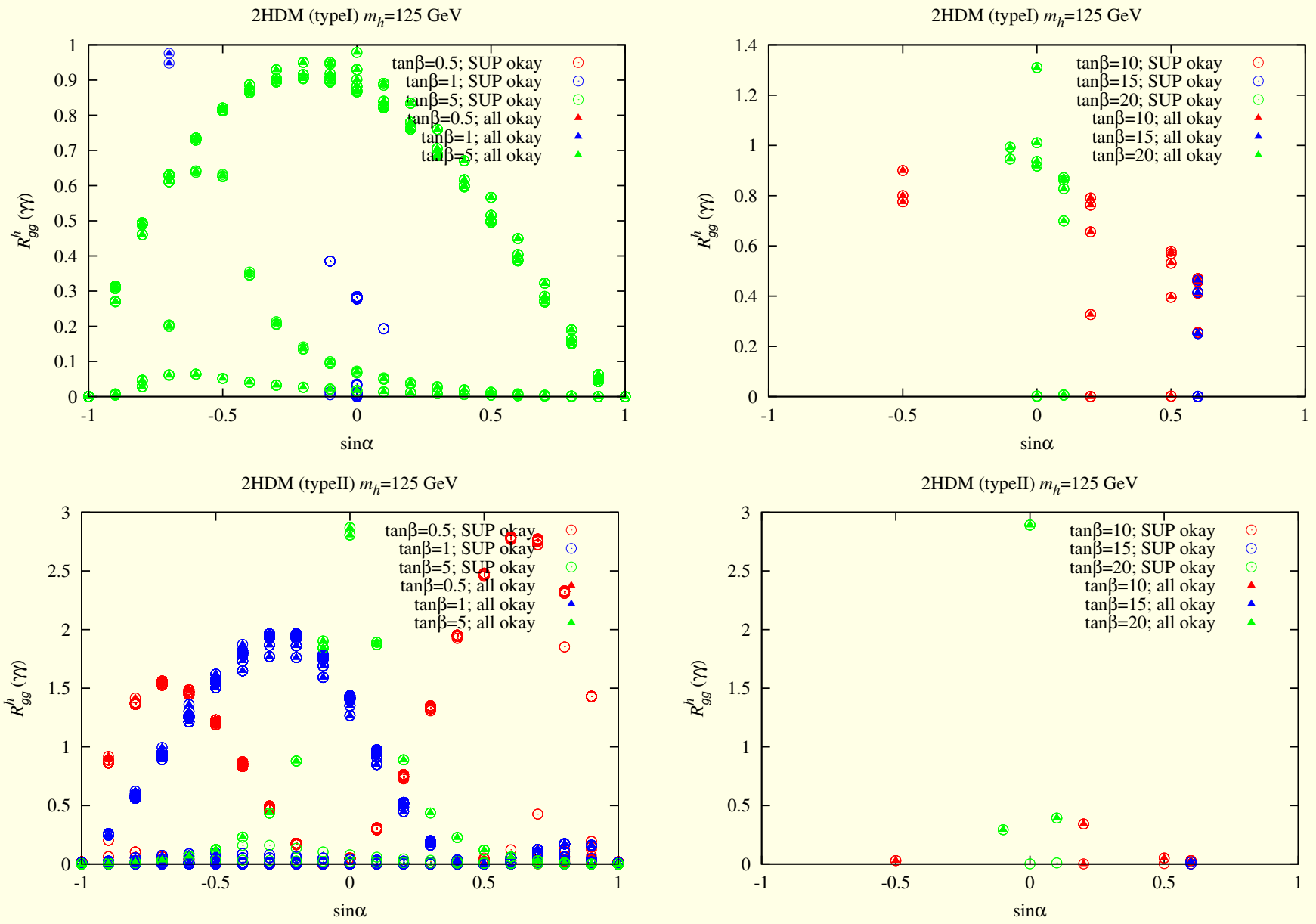

Figure 14: $R^h_{gg}(\gamma\gamma)$ is plotted as a function of $\sin\alpha$ for a sequence of $\tan\beta$ values. Different constraint combinations are considered and the different curves of given type correspond to a variety of other input parameters. The upper plots are for the Type I model and the lower plots are for the Type II model. Different colors indicate different $\tan\beta$ values.

Conclusions on the 2HDM, type I and II setup:

- Easier to enhance $R_{gg}^{h_i}$ for the type II model:
  - $R_{gg\ \max}^{h_i\ \text{type II}}(\gamma\gamma) \lesssim 3-4$,
  - $R_{gg\ \max}^{h_i\ \text{type I}}(\gamma\gamma) \lesssim 2-3$.

- Type II model implies too strong ZZ signal:

$$1 < R_{gg\ \max}^{h_i\ \text{type II}}(\gamma\gamma) \lesssim R_{gg\ \max}^{h_i\ \text{type II}}(ZZ) \sim 2-3.5$$

- Optimal signal for the type I model for $\tan\beta = 4, 20$ within the scenarios: I ($m_h = 125$ GeV) and IV ($m_h = m_A = 125$ GeV).

- $H^{\pm}$ effects up to $\sim 20\%$.

Summary

- The off-brane RS scenario with R-Higgs mixing:
  - A realistic explanation for the recent LHC data for a signal at only 125 GeV, e.g. $m_0/m_{Pl} = 0.4$ and $\xi \sim -0.09$.
  - No consistent solution for a signal (h or ϕ) at 125 GeV and high mass.

- 2HDM's type I and II:
  - Consistent fit to the signal seen at the LHC. Data seem to favour the type I model with $\tan\beta = 4, 20$ $m_H = 225$ GeV, $m_A = 200$ GeV, $m_{H^\pm} = 90$ GeV, $m_{12} = 100, 50$ GeV and $\sin\alpha = -0.1, 0.0$.